


Multidelay pseudocontinuous arterial spin labeling to measure blood flow in the head and neck

Nienke D. Sijtsema^{1,2}  | Steven F. Petit¹ | Gerda M. Verduijn¹ |
Dirk H. J. Poot² | Esther A. H. Warnert^{1,2} | Mischa S. Hoogeman^{1,3} |
Juan A. Hernandez-Tamames²

¹Department of Radiotherapy, Erasmus MC Cancer Institute, University Medical Center Rotterdam, Rotterdam, The Netherlands

²Department of Radiology and Nuclear Medicine, Erasmus MC, University Medical Center Rotterdam, Rotterdam, The Netherlands

³Department of Medical Physics and Informatics, HollandPTC, Delft, The Netherlands

Correspondence

Nienke D. Sijtsema, Department of Radiotherapy, Erasmus MC Cancer Institute, PO Box 2040, 3000 CA, Rotterdam, The Netherlands.

Email: n.sijtsema@erasmusmc.nl

Funding information

This work was funded by a research grant from Elekta AB (Stockholm, Sweden).

Perfusion MRI is promising for the assessment, prediction, and monitoring of radiation toxicity in organs at risk in head and neck cancer. Arterial spin labeling (ASL) may be an attractive alternative for conventional perfusion MRI, that does not require the administration of contrast agents. However, currently, little is known about the characteristics and performance of ASL in healthy tissues in the head and neck region. Therefore, the purpose of this study was to optimize and evaluate multidelay pseudocontinuous ASL (pCASL) for the head and neck region and to explore nominal values and measurement repeatability for the blood flow (BF), and the transit time and T1 values needed for BF quantification in healthy tissues. Twenty healthy volunteers underwent a scan session consisting of four repeats of multidelay pCASL (postlabel delays: 1000, 1632, 2479 ms). Regions of interest were defined in the parotid glands, submandibular glands, tonsils, and the cerebellum (as a reference). Nominal values of BF were calculated as the average over four repeats per volunteer. The repeatability coefficient and within-subject coefficient of repeatability (wCV) of BF were calculated. The effect of T1 (map vs. cohort average) and transit time correction on BF was investigated. The mean BF (\pm SE) was 55.7 ± 3.1 ml/100 g/min for the parotid glands, 41.2 ± 2.8 ml/100 g/min for the submandibular glands, and 32.3 ± 2.2 ml/100 g/min for the tonsils. The best repeatability was found in the parotid glands (wCV = 13.3%–16.1%), followed by the submandibular glands and tonsils (wCV = 20.0%–24.6%). On average, the effect of T1 and transit time correction on BF was limited, although substantial bias occurred in individual acquisitions. In conclusion, we demonstrated the feasibility of BF measurements in the head and neck region using multidelay pCASL and reported on nominal BF values, BF repeatability, the effect of T1, and transit time in various tissues in the head and neck region.

KEYWORDS

arterial transit time, head and neck, multidelay pseudocontinuous arterial spin labeling, perfusion, repeatability, T1 map

Abbreviations used: 3D-QALAS, three-dimensional multiparametric quantification using an interleaved Look–Locker acquisition sequence with a T2 preparation pulse; ASL, arterial spin labeling; BF, blood flow; DCE, dynamic contrast enhanced; DSC, dynamic susceptibility contrast; LD, labeling duration; pCASL, pseudocontinuous arterial spin labeling; PLD, postlabeling delay; RC, repeatability coefficient; ROI, region of interest; SAR, specific absorption rate; SMG, submandibular gland; wCV, within-subject coefficient of variation; wSD, within-subject standard deviation.

This is an open access article under the terms of the [Creative Commons Attribution-NonCommercial](https://creativecommons.org/licenses/by-nc/4.0/) License, which permits use, distribution and reproduction in any medium, provided the original work is properly cited and is not used for commercial purposes.

© 2023 The Authors. *NMR in Biomedicine* published by John Wiley & Sons Ltd.

1 | INTRODUCTION

Perfusion phenomena in tissues can be assessed by a number of techniques, including dynamic contrast enhanced (DCE) MRI, dynamic susceptibility contrast (DSC) MRI, and arterial spin labeling (ASL). Yet, while DCE and DSC have found their way into state-of-the-art imaging protocols for the head and neck region,¹ ASL has only recently gained more attention for the head and neck region.² The advantage of ASL is that, in contrast to DCE and DSC, it does not require the injection of an external contrast agent. Recently, the potential value of ASL in head and neck cancer has been demonstrated for the detection of residual tumor after treatment,³ differentiating between tumor types,^{4,5} determining tumor stage,⁶ differentiation between benign and malignant tissue,⁷ differentiation between metastatic and reactive lymph nodes,⁸ and even early treatment response.⁹ In general, a good correlation between blood flow (BF) values measured by DCE and ASL^{10,11} is reported.

However, to date, the overwhelming majority of research on ASL in the head and neck region has focused on the tumor. Besides the tumor, perfusion MRI may have added value in the assessment, prediction, and monitoring of toxicity of the (chemo)-radiotherapy treatment in important organs at risk in the head and neck. For example, changes in the perfusion during treatment have been observed with DCE in submandibular and parotid glands.^{12,13} Avoiding the administration of a contrast agent, especially when sessions are repeated during treatment, would be preferable, hence the interest in ASL for normal tissues in the head and neck region.

Currently, ASL for the head and neck is under development, and very little is known about BF values and T1 in healthy tissues in the head and neck region, transit times of the blood to these tissues, and the repeatability of the BF values. Moreover, normative values are important to help put BF values and BF changes in patients into perspective; they also provide essential information for the design of (clinical) studies to analyze the normal tissue response to treatment and possible the incorporation of ASL into clinical protocols in the future.

Therefore, the aim of this study was to optimize and evaluate a multidelay pseudocontinuous ASL (pCASL) sequence and explore nominal BF values for several tissues in the head and neck region. To this end, we investigated the repeatability of BF, obtained T1 values of the tissues, and investigated the influence of transit time correction and T1 value on BF measurements.

2 | MATERIALS AND METHODS

2.1 | Subjects

In total, 20 healthy subjects were included (mean age 25 years, age range 20–31 years, nine males, 11 females). This study was approved by our institutional medical ethical board (protocol 2014–096) and written informed consent was obtained from all subjects. Exclusion criteria were any metal-containing implants, fillings, or braces, in or around the oral cavity.

2.2 | Imaging protocol

All subjects were scanned on a 3-T MR750 Discovery system (GE Healthcare, Waukesha, WI, USA) with a 12-channel head and neck coil (GE Healthcare). The scan protocol consisted of a three-dimensional (3D) multiparametric quantification using an interleaved Look-Locker acquisition sequence with a T2 preparation pulse (3D-QALAS), three-delay encoded ASL, and multi b-value diffusion-weighted imaging. The 3D-QALAS¹⁴ (0.5 × 0.5 × 2 mm³ voxels, scan time 4 min 4 s) scan was acquired in the axial plane. The SyMRI version 0.45.2721Q1 software package (SyntheticMR AB, Linköping, Sweden) was used to generate synthetic T1-weighted, T2-weighted, and proton density-weighted images, and a T1 map was used for quantification of the ASL BF. Next, a 3D encoded pCASL scan was acquired that incorporated three postlabel delays (PLDs) in one acquisition^{15,16} (3D stack of spirals fast spin echo with six arms, PLDs: 1000, 1632, 2479 ms, total labeling duration [LD]: 3000 ms, effective LD per PLD: 632 ms [PLD = 1000 ms], 847 ms [PLD = 1632 ms], 1521 ms [PLD = 2479 ms], 2.2 × 2.2 × 4 mm³ voxels, 128 × 128 × 26 matrix [acquired resolution], TE = 10.5 ms, TR = 6012 ms, number of averages = 2, scan time 5–7 min). Background suppression was implemented according to Maleki et al.¹⁷ The labeling plane was automatically placed 2 cm below the most caudal slice, which was positioned on the chin, to ensure the labeling plane was situated in the neck area (Figure 1). All ASL scans were acquired in the axial plane, and the subjects were positioned in the scanner as straight as possible (i.e., left and right symmetry in the axial plane), such that the labeling plane was, by approximation, perpendicular to the BF direction for all volunteers. Padding was used to minimize involuntary motion during the scan session. A three-delay pCASL was chosen as this is a robust protocol that would be suitable for a variety of tissues in the head and neck region. The three-delay pCASL scan was repeated four times while the subject remained in the scanner, with intervals of 5 min. The total scan time for each subject was 1 h.

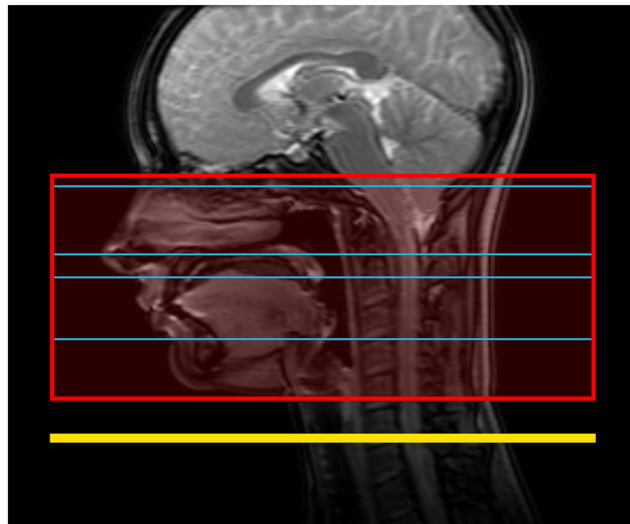


FIGURE 1 Example of the placement of the field of view (red) and labeling plane (yellow) for one volunteer; the blue lines indicate the slices, as displayed in Figure 2. The labeling plane was automatically placed 2 cm below the most caudal slice of the field of view.

2.3 | Postprocessing

2.3.1 | Organs of interest

The study focused on the parotid glands and submandibular glands because these are important organs at risk in head and neck radiotherapy treatments. In addition, the tonsils were added to represent a surrogate tumor location, to assess the feasibility of measuring BF in healthy tissue and tumor simultaneously in one comprehensive ASL protocol. All tissues of interest were delineated by an experienced radiation oncologist on the synthetic T2-weighted images obtained from 3D-QALAS. Because ASL in brain has been described extensively, a region of interest (ROI) was also drawn in the cerebellum as a reference measurement to compare with previous literature. Each ASL scan was rigidly registered to the synthetic proton density-weighted image from 3D-QALAS, because the proton density-weighted contrast is most similar to the 2-s saturation recovery image from the ASL sequence. Subsequently, delineations were transferred to each ASL acquisition. To diminish the influence of delineation errors, registration errors, and the partial volume effect, so that only the tissue of interest is contained within the contours, the 3D delineated volumes of the parotid glands, submandibular glands, and the tonsils were eroded by 2 mm in the axial plane and by 4 mm in the slice direction. The eroded contours are referred to as the ROIs. The cerebellum ROI was not eroded, because the cerebellum was not delineated, but an ROI was drawn inside the cerebellum instead.

2.3.2 | ASL BF quantification

To avoid bias because of an imperfectly chosen PLD, the BF was transit time corrected through voxel-wise fitting of the ASL signal to Equation (1) using the three PLDs.¹⁵ Fitting was performed for the ROI of each tissue of interest separately.

$$BF = \frac{6000 \lambda e^{\delta/T1_a}}{2eT1_t \left(e^{\frac{\max(PLD-\delta,0)}{T1_t}} - e^{\frac{\max(LD+PLD-\delta,0)}{T1_t}} \right)} \frac{SI_{PW}}{S_c} \quad (1)$$

where SI_{PW} is the signal intensity of the perfusion-weighted image and SI_{SR} is the signal intensity in the 2-s saturation-recovery image of the ASL acquisition, which is divided by a factor $S_c = 1 - e^{-\frac{2}{T1_t}}$ to correct for partial signal recovery. δ , the arterial transit time, is estimated by the signal-weighted delay method, as described by Dai et al.¹⁵ λ is the blood-tissue partition coefficient, which was set to 0.9 g/ml. e is a correction factor to account for the combined effect of labeling efficiency and background suppression and was set to 0.6 to conform to the manufacturer's guidelines. $T1_a$ is the T1 of arterial blood and was set to 1650 ms.^{18,19} $T1_t$ is the T1 of the tissue of interest and, unless specifically stated otherwise, was incorporated voxel-wise based on the T1 map obtained from QALAS.

2.4 | Assessment

2.4.1 | Nominal values of BF

Although BF values are by definition positive, the BF estimated by Equation (1) can be negative because of noise or motion causing misalignment between the control and labeled images. In the ROIs, the voxels containing a negative BF were excluded. Therefore, the mean BF was determined in each repeated acquisition only over those voxels containing a positive BF. Next, the mean BF per subject (\overline{BF}_s) was calculated per tissue by averaging over the four repeats. The nominal values of the BF in the tissues were defined by $\overline{BF}_n \pm SD$, where \overline{BF}_n is the grand mean over the \overline{BF}_s for the left and right side combined of each tissue for all subjects (i.e., 40 measurements in total per tissue) and its corresponding standard deviation (SD) and standard error (SE). The range of ROI means of all subjects and repeats is reported for each tissue of interest, as well as being plotted per subject. Because T1 values of the tissues were necessary for the quantification of BF, the range of T1 values of the tissues are reported. The \overline{BF}_s and T1 were compared between the parotid glands, submandibular glands, and the tonsils (left and right averaged) using a paired Students *t*-test in R statistical software (version 4.1.2, R Foundation for Statistical Computing, Vienna, Austria). Because of the limited number of comparisons (six in total), *p* values were not corrected for multiple comparisons and a *p* value less than 0.05 was considered statistically significant.

2.4.2 | Repeatability

To calculate the repeatability measures, the within-subject SD (wSD) of the ROI mean was estimated for each tissue of interest by fitting a linear mixed effect model where the ROI means (one per repeat per ROI) were grouped by subject. For this purpose, the lme4 package (version 1.1-27.1)²⁰ in R statistical software (version 4.1.2, R Foundation for Statistical Computing) was used. Next, the repeatability coefficient (\widehat{RC})²¹, which indicates the minimum true difference, was calculated, using

$$\widehat{RC} = 1.96 \sqrt{2} wSD \approx 2.77 wSD. \quad (2)$$

The within-subject coefficient of variation was calculated as well, as this relative measure eases comparison of repeatability between tissues:

$$wCV = \frac{wSD}{\overline{BF}_t}, \quad (3)$$

where \overline{BF}_t is the nominal BF per tissue, left and right separated.

2.4.3 | Influence of T1 and PLD

The average T1 per tissue over all volunteers was calculated to investigate the influence of T1 on the BF measurement, and to assess whether the acquisition of a T1 map could be omitted by using an average T1 in the BF estimation. For the parotid glands, submandibular glands, and the tonsils, the left and right measurements were grouped before calculation of the average, so the average T1 was based on 40 ROI means for these tissues. A new BF map was constructed for each tissue according to Equation (1), with the exception that the $T1_t$ was set to the group average per tissue before voxel-wise fitting of the ASL signal, instead of using the T1 map. The difference between the BF based on the fixed T1 and based on the T1 map was calculated for each acquisition, plotted and reported, to assess the possible bias in BF estimation if a T1 map is not available. Additionally, the wCV and RC were calculated for the BF based on a fixed T1 and compared with the wCV and RC calculated for the T1 map-based BF.

To investigate the possible underestimation of BF when using only one PLD, the BF was calculated voxel-wise according to the following equation for each PLD separately without transit time correction:

$$BF = \frac{6000 \lambda e^{PLD/T1_a} S_{IPW}}{2eT1_t \left(1 - e^{-\frac{PLD}{T1_t}}\right) \frac{S_{ISR}}{S_c}}. \quad (4)$$

The difference between the three nontransit time-corrected BF values based on each of the three single PLDs and the transit time-corrected BF was calculated for each pCASL acquisition, then plotted and reported.

3 | RESULTS

Out of 20 volunteers, five had undergone resection of their tonsils and one presented only the right tonsil on the synthetic T1w and T2w scans. Therefore, the right tonsil was assessed in 15 volunteers and the left tonsil was assessed in 14 volunteers in total. Additionally, one repeat scan from one volunteer was fully excluded because of specific absorption rate (SAR) limitations. The size of the ROIs (i.e., after erosion in the case of the parotid glands, submandibular glands, and the tonsils) (\pm SD) was 6.8 ± 3.1 (range 2.0–15.9) cc for the parotid glands, 1.9 ± 0.7 (0.5–3.3) cc for the submandibular glands, 0.5 ± 0.5 (0.1–1.7) cc for the tonsils, and 11.6 ± 4.2 (5.7–21.9) cc for the cerebellum. The percentage of negative voxels that were excluded was 0.4% for the left parotid gland, 2.1% for the right parotid gland, 2.1% for the left submandibular gland, 3.8% for the right submandibular gland, 0.1% for both tonsils, and 0.7% for the cerebellum.

Figure 2 shows an example of the delineations (before erosion) of the tissues in the head and neck region in several slices on the synthetic T2w image, T1 map, and BF map. The average T1 in the ROI ranged from 833 to 1645 ms for the parotid glands, 1079 to 1876 ms for the submandibular glands, and 1955 to 2892 ms for the tonsils, and was significantly different for these three tissues (Figure 3A). Table 1 shows the nominal values for the BF in the tissues in the head and neck, with their SD (which reflects the between subject variability) and SE. BF was significantly different between the parotid glands, submandibular glands, and the tonsils (Figure 3B). As can be seen in Figure 3B, the ranges of BF in the tissues on the left and on the right generally coincided well. The mean BF for the right parotid gland ranged from 33.9 to 87.2 ml/100 g/min, while for the left parotid gland it ranged from 36.1 to 90.0 ml/100 g/min. For the right submandibular gland, the range was from 20.6 to 61.6 ml/100 g/min, while for the left it was from 21.0 to 80.6 ml/100 g/min. For the right tonsil, the range was from 15.8 to 44.9 ml/100 g/min, while for the left it was from 14.8 to 45.8 ml/100 g/min. However, the median BF for the left tonsil was higher than that for the right tonsil.

In general, all the tissues in the head and neck displayed similar transit times, on average (\pm SD), 1177 ± 76 ms for the right parotid gland, 1179 ± 66 ms for the left parotid gland, 1287 ± 165 ms for the right submandibular gland, 1204 ± 77 ms for the left submandibular gland, 1204 ± 128 ms for the right tonsil, and 1205 ± 119 ms for the left tonsil. However, the transit time for the cerebellum was notably longer, on average, 1715 ± 170 ms. This is graphically depicted in Figure S1.

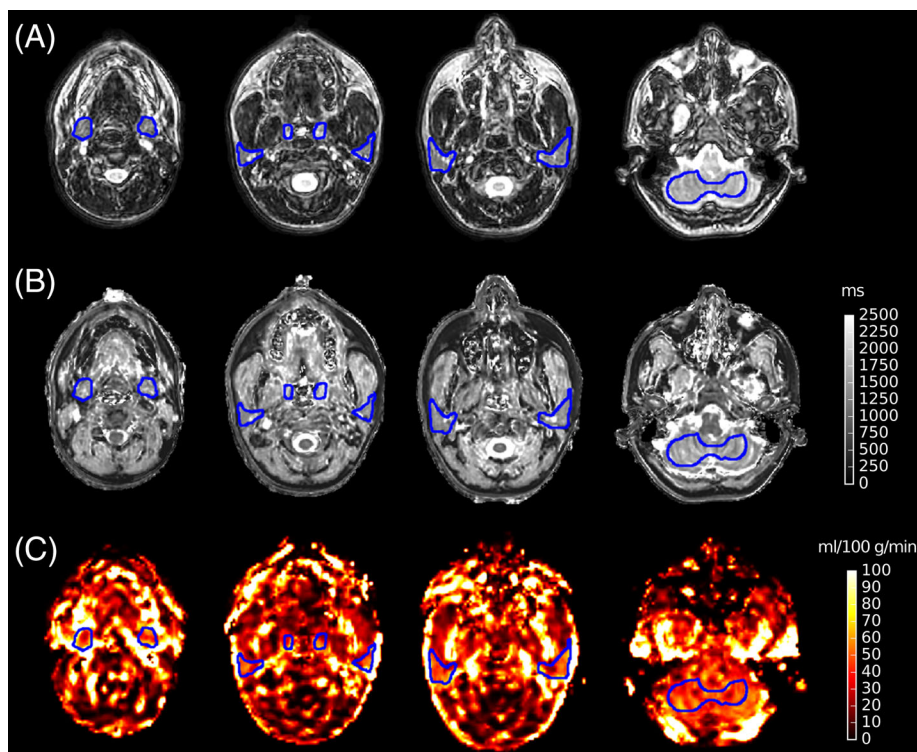


FIGURE 2 Example of the (A) T2w image, (B) T1 map, and (C) BF map for three different slices in one volunteer. Delineations (i.e., before erosion) are shown for the submandibular glands (first column), the tonsils (the two medial ROIs in the second column), and the parotid glands (third column). The cerebellum ROI is shown in the last column. The location of each of the slices is also indicated by blue lines in Figure 1. Note that delineations of the parotid glands are also visible in the third column. BF, blood flow; ROI, region of interest.

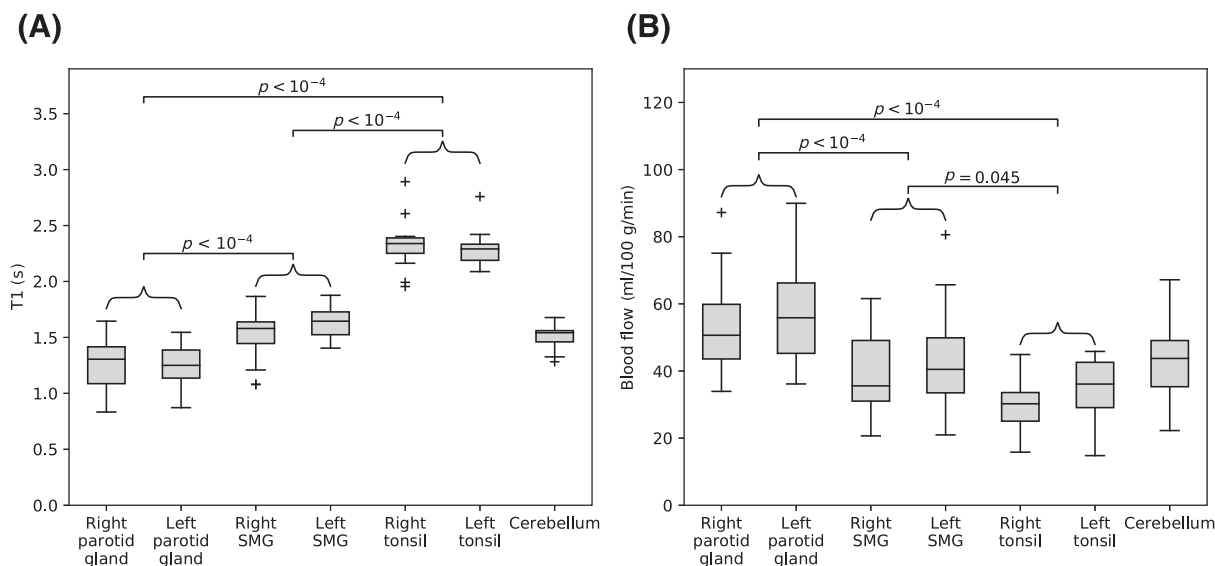


FIGURE 3 (A) Boxplot of the mean T1 for each tissue of interest per volunteer. Tonsils have a notably higher T1 than the other tissues, probably caused by high water content. Additionally, the range of T1 in the parotid glands is notably larger than in the other tissues. (B) Boxplot of the mean BF per volunteer (mean over the repeats) for each of the tissues of interest. The parotid glands showed the highest perfusion, while the tonsils displayed the lowest perfusion. For both (A) and (B), a paired *t*-test with the tonsils was performed with $n = 14$, because some volunteers did not present with both tonsils, while comparisons between the parotid and submandibular glands were performed with $n = 20$. BF, blood flow; SMG, submandibular gland.

TABLE 1 Nominal values of BF with corresponding SD and SE.

Tissue	BF (ml/100 g/min)	SD	SE
Parotid glands ($n = 20$)	55.7	14.0	3.1
Submandibular glands ($n = 20$)	41.2	12.4	2.8
Tonsils ($n = 14$)	32.3	8.1	2.2
Cerebellum ($n = 20$)	43.0	10.7	2.4

Abbreviations: BF, blood flow; SD, standard deviation; SE, standard error.

Figure 4 shows plots of the mean BF per repeat per volunteer in the parotid glands, submandibular glands, tonsils, and the cerebellum. The majority of the ranges overlapped for the left and right sides for all tissues. However, no overlap of the range of measurements between the left and right sides was present in two volunteers in the parotid glands, in two volunteers in the submandibular glands, and in three volunteers in the tonsils.

Table 2 shows the repeatability of measurements. The best relative repeatability in terms of wCV was obtained in the cerebellum (9.0%), followed by the parotid glands (13.3%–16.1%). The tonsils and submandibular glands showed similar repeatability (20.0%–24.6%).

The average T1 (\pm SD) derived and used as a fixed T1 was 1255 ± 218 ms for the parotid glands, 1584 ± 188 ms for the submandibular glands, 2317 ± 191 ms for the tonsils, and 1506 ± 101 ms for the cerebellum. While the median difference between using a T1 map, compared with a fixed T1, was close to zero in all cases, for individual acquisitions the difference in BF ranged from -34 to 23 ml/100 g/min for the parotid glands, from -23 to 8 ml/100 g/min for the submandibular glands, from -14 to 5 ml/100 g/min for the tonsils, and from -9 to 8 ml/100 g/min for the cerebellum. This is also shown in Figure S2. The repeatability of the BF measurements based on the fixed T1 was similar to the repeatability of BF estimated using a T1 map. Table S1 shows the wCV and RC for the fixed T1 approach.

For the parotid glands, notable underestimation of the BF (i.e., zero difference is on the edge or outside the 25%–75% percentile range) was present for all three PLDs when comparing nontransit time-corrected BF with transit time-corrected BF. Notable underestimation of BF was present in the submandibular glands and the left tonsil for the longest PLD (2479 ms) only. For the cerebellum, underestimation was present for the two shortest PLDs (1000 and 1632 ms), but not for the longest PLD. The errors in BF when no transit time correction was applied are also shown in Figure S3.

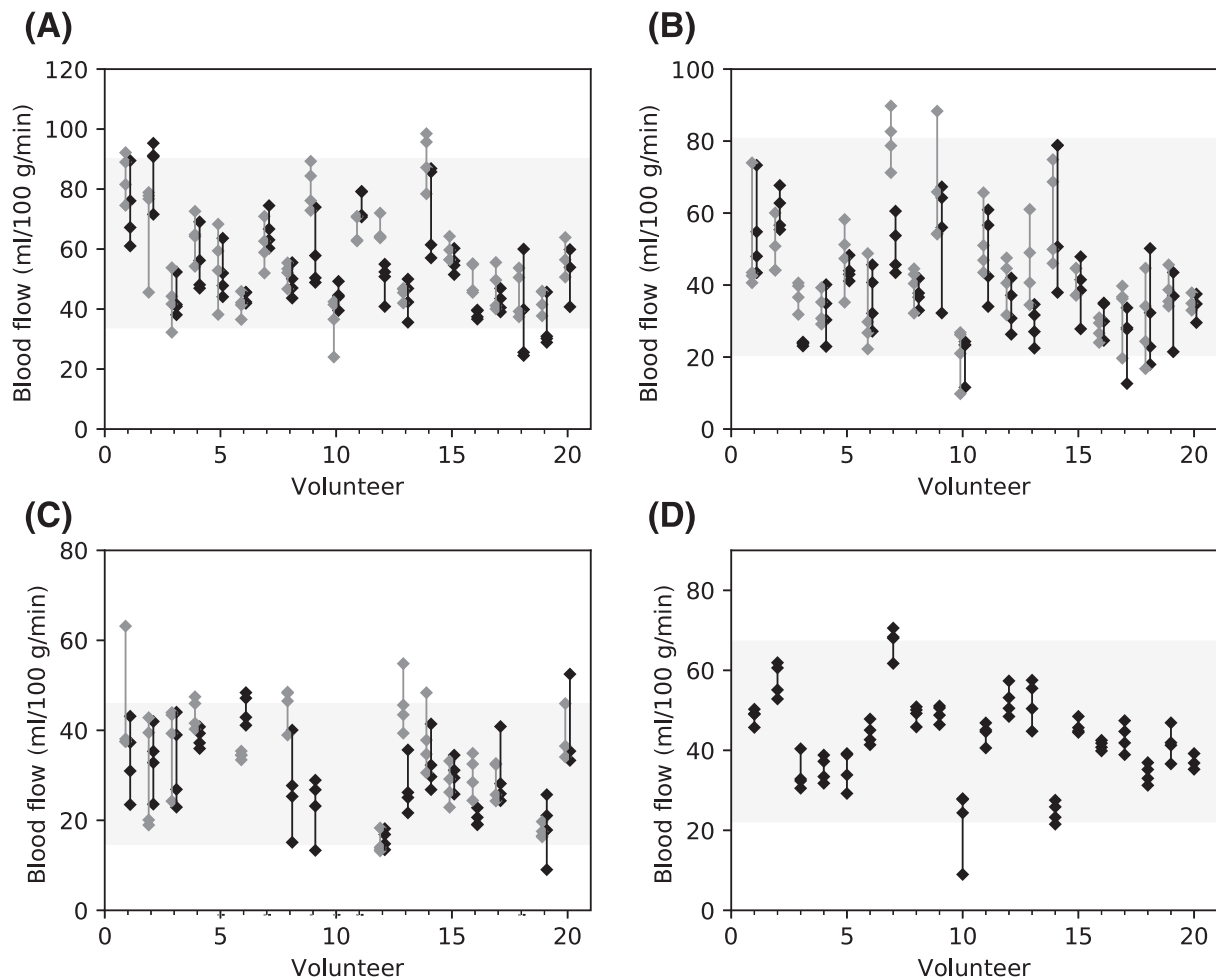


FIGURE 4 Plot showing the BF measurement for each acquisition for (A) The parotid glands, (B) The submandibular glands, (C) The tonsils, and (D) The cerebellum. The left side is denoted in gray and the right side in black (if applicable). The gray box indicates the minimum and maximum values of the mean BF per volunteer (shown as the extent of the boxplot in Figure 3B), with the left and right combined (if applicable). BF, blood flow.

TABLE 2 Repeatability measures of BF for the assessed tissues.

Tissue	RC (95% CI) (ml/100 g/min)	wCV (–)
Parotid gland, right	23.9 (20.2, 29.0)	16.1%
Parotid gland, left	21.3 (18.0, 25.9)	13.3%
SMG, right	26.7 (22.5, 32.4)	24.6%
SMG, left	26.1 (22.0, 31.6)	21.8%
Tonsil, right	18.8 (15.4, 23.5)	22.8%
Tonsil, left	18.8 (15.4, 23.8)	20.0%
Cerebellum	10.7 (9.0, 13.0)	9.0%

Abbreviations: BF, blood flow; CI, confidence interval; RC, repeatability coefficient; SMG, submandibular gland; wCV, within-subject coefficient of variation

4 | DISCUSSION

ASL is a perfusion MRI technique of interest for the prediction and monitoring of tumor and healthy tissue response to head and neck (chemo-) radiotherapy, with the advantage, especially in the case of repeated examinations, that no external contrast agent is necessary. However, literature on ASL in the head and neck region remains scarce. To gain insight into the applicability of ASL in the head and neck area, we derived the nominal values and repeatability of the BF obtained from multidelay pCASL in a variety of tissues in 20 healthy volunteers. We found the average BF in the parotid glands to be the highest (range 33.9–90.0 ml/100 g/min) out of the assessed tissues in the head and neck, with the best wCV

(13.3%–16.6%). The submandibular glands (range 20.6–80.6 ml/100 g/min) and the tonsils (range 14.8–45.8 ml/100 g/min) had a lower BF. The wCV of the tonsils and submandibular glands were similar, ranging from 20.0% to 24.6%.

The ROI in the cerebellum showed values of BF and T1 that agreed with previously published literature.^{22,23} When comparing the repeatability in terms of wCV between the cerebellum and the other tissues, the cerebellum had notably better repeatability. One explanation for this could be the presence of motion in the neck region caused by breathing, swallowing, or jaw movement, which would have affected the tonsils and submandibular glands and parotid glands, but not the cerebellum. The development of more motion robust, or motion correction for this type of ASL sequences, could therefore be of interest for future research. Another explanation for the varying repeatability across tissues could be the size of the ROIs, where the influence of noise on the ROI average is less for the large cerebellum ROI than for the small tonsil ROI.

The estimated repeatability coefficients were in the range of 18–27 ml/100 g/min depending on the tissue, so if a difference smaller than the RC is detected, it might not be a true difference. Although the RC was relatively high (in the range of 15%–20% of the mean) compared with the absolute values of BF, differences between volunteers in the order of the estimated RC were observed. Additionally, the differences in BF between benign and malignant, or residual tumor and local control cases reported in previous publications, are in the range of the RC found in this study or larger. For example, Abdel Razek²⁴ reported an average difference between benign and malignant parotid lesions of 33.4 ml/100 g/min, which is similar to the RC we estimated for the parotid glands. Fujima et al.³ reported an average difference of 28.5 ml/100 g/min when comparing residual tumor with the case with local control after treatment of head and neck squamous cell carcinoma. Furthermore, they also reported an average reduction (of 96.5 ml/100 g/min) in BF from an average tumor BF of 121.4 ± 27.8 ml/100 g/min pretreatment to an average tumor BF of 24.9 ± 14.9 ml/100 g/min posttreatment. Because this change in BF is substantially larger than the observed RC, this suggests the repeatability is sufficient to assess BF changes in a treatment setting.²¹ However, in the current study, we obtained intrasession measurements of BF, and therefore we could not assess the stability of BF over the course of a few weeks, a similar time frame to treatment.

The range in average BF measured over the volunteers was approximately the same for the left and right side for the different organs. However, the left tonsil showed a slightly larger BF on average. This is most likely an effect of the three volunteers who displayed a higher BF (≥ 10 ml/100 g/min) in the left compared with the right tonsil. In a substantial number of volunteers (10%–20%), the range of BF values found did not overlap between the left and right for each of the three organs in the head and neck region. However, in these cases, the absolute differences were smaller than the estimated RC, and therefore it cannot be concluded that this is a true difference. While eroding the delineation of the tissues most likely diminished the influence of delineation and matching uncertainty, subtle differences in the ROIs could still lead to substantial differences in BF measurements, especially in the presence of vessels, such as in the parotid glands. Additionally, the subjects were carefully positioned as straight as possible in the scanner. However, small differences between left and right might still arise from positioning variation.

The T1 value of the tissue of interest highly affected BF quantification. As we show in this study, T1 can vary substantially between tissues, and therefore it is important to use a suitable T1 for each of the tissues. Using a T1 map for this purpose yields a personalized voxel-wise T1, but T1 maps can introduce additional noise into the BF measurements. Using a fixed cohort-average value of T1 for each of the tissues did not yield substantial average bias in BF compared with using a T1 map. However, substantial individual differences were still observed. It is unclear if the benefit of reduced bias (compared with a fixed T1) when using a T1 map outweighs the increased variance of BF measurements because of the introduction of extra noise through the T1 map.

The average transit times we found for each of the tissues in the head and neck region were similar, which suggests that it is sufficient to assess the BF in these tissues simultaneously with only one PLD without introducing substantial bias to the BF measurements, in which case a PLD between 1000 and 1632 ms would be the most appropriate. Assessing these tissues with one PLD provides an opportunity to acquire more averages within the same scan time, and therefore yield a more stable BF measurement. Still, individual measurements can deviate substantially, especially when an ROI contains multiple tissue types. However, from these results it is unclear whether this is caused by uncertainties in the transit time measurements, or because of variations in the signal-to-noise ratio or effective label duration, or is attributable to true variation in BF. Additionally, to address other areas, like base of skull malignancies, which are closer to the cerebellum and for which the transit times are longer, then another PLD would be required. It should be noted, however, that the positioning of the labeling plane plays an important role in the expected transit time.

Given the proximity to the feeding arteries, it is necessary to choose a short PLD. We chose a minimum PLD of 1000 ms, similar to Lin et al.,²⁵ and lower than most other reported PLDs for the head and neck region.² However, because of shorter distances between the arteries and the labeling plane, and the target tissues, the optimal PLD may vary.² So a limitation of this study is that no PLDs below 1000 ms were used, because of the large vascular artifacts we observed at lower PLDs. A minimum PLD of 1000 ms could not fully avoid vascular artifacts because of the many large vessels supplying the head, neck, and brain. Therefore, vascular artifacts could have potentially influenced the BF quantification. Additionally, no upper limit for the BF was used in the analyses, therefore, it is possible that intra-arterial signal could have influenced the BF quantification. In the future, taking account of the arterial component by using a two-compartment model could present a solution to this problem.²⁶

To exclude the nonphysiological result of a negative BF, voxels containing negative BF were excluded from the analysis. As demonstrated in Tables S2 and S3, including voxels with a negative BF would have led to a deterioration of repeatability, while the nominal BF values were hardly affected (maximum deviation < 2.2 ml/100 g/min, which was well within one SE).

In the current analysis, full perfusion maps were constructed and, subsequently, ROI averages were computed. Because of the nonlinear model fitting, this approach is probably more susceptible to acquisition noise than performing the model fitting on ROI-averaged signals. However, that would assume homogeneous tissues, which we did not want to assume, because of the intended application of imaging tumors, which are, in general, heterogeneous structures.

In this work, a blood–tissue partition coefficient (λ) of 0.9 was used, as is customarily used for brain imaging. However, a value of 1 was also previously used in a study in head and neck cancer.^{3,27} Because the estimated BF scales linearly with λ , an error in λ of 10% yields an error of 10% in BF as well. However, it could be that the tissues assessed in this study have different values for λ , as λ is known to vary per age, tissue, subject, and pathology.^{28,29}

Finally, the volunteers in this cohort were all healthy, young volunteers. BF can be influenced by several diseases and may deviate by age. Therefore, caution should be taken when translating these values to other cohorts. Additionally, expanding the cohort would have likely resulted in a smaller SE of the mean. However, the gain in SE would most likely be limited because currently it is around 5% of the mean.

5 | CONCLUSION

We demonstrated the feasibility of using multidelay pCASL to simultaneously measure BF in several tissues in the head and neck region. Moreover, we presented nominal BF values for the parotid glands, submandibular glands, and tonsils. While some variation in BF was found between different subjects, generally the parotid glands were the most perfused and the tonsils the least perfused. Additionally, we have also reported the average values of T1 needed for BF quantification for the tissues assessed, which, to the best of our knowledge, have not been reported before. The results suggest that the repeatability of the BF measurements we found is sufficient for these measurements to be included in clinical studies regarding tumor detection, and treatment and toxicity monitoring.

ACKNOWLEDGMENTS

The authors would like to thank Kazem Nasserinejad, PhD, for his help with the statistical analysis. This work was funded by a research grant from Elekta AB (Stockholm, Sweden).

CONFLICT OF INTEREST

Erasmus MC Cancer Institute also has research collaborations with Accuray Inc. (Sunnyvale, CA, USA) and Varian, a Siemens Healthineers Company (Palo Alto, CA, USA).

ORCID

Nienke D. Sijtsema  <https://orcid.org/0000-0001-7928-1578>

REFERENCES

- Manfrini E, Smits M, Thust S, et al. From research to clinical practice: a European neuroradiological survey on quantitative advanced MRI implementation. *Eur Radiol*. 2021;31(8):6334–6341. doi:10.1007/s00330-020-07582-2
- Martin-Noguerol T, Kirsch CFE, Montesinos P, Luna A. Arterial spin labeling for head and neck lesion assessment: technical adjustments and clinical applications. *Neuroradiology*. 2021;63(12):1969–1983. doi:10.1007/s00234-021-02772-1
- Fujima N, Kudo K, Yoshida D, et al. Arterial spin labeling to determine tumor viability in head and neck cancer before and after treatment. *J Magn Reson Imaging*. 2014;40(4):920–928. doi:10.1002/jmri.24421
- Kato H, Kanematsu M, Watanabe H, et al. Perfusion imaging of parotid gland tumours: usefulness of arterial spin labeling for differentiating Warthin's tumours. *Eur Radiol*. 2015;25(11):3247–3254. doi:10.1007/s00330-015-3755-7
- Yamamoto T, Kimura H, Hayashi K, Imamura Y, Mori M. Pseudo-continuous arterial spin labeling MR images in Warthin tumors and pleomorphic adenomas of the parotid gland: qualitative and quantitative analyses and their correlation with histopathologic and DWI and dynamic contrast enhanced MRI findings. *Neuroradiology*. 2018;60(8):803–812. doi:10.1007/s00234-018-2046-9
- Abdel Razeq AAK, Nada N. Arterial spin labeling perfusion-weighted MR imaging: correlation of tumor blood flow with pathological degree of tumor differentiation, clinical stage and nodal metastasis of head and neck squamous cell carcinoma. *Eur Arch Otorhinolaryngol*. 2018;275(5):1301–1307. doi:10.1007/s00405-018-4950-3
- Li Y, Li X, Yu X, et al. Investigating the value of arterial spin labeling and intravoxel incoherent motion imaging on diagnosing nasopharyngeal carcinoma in T1 stage. *Cancer Imaging*. 2020;20(1):62. doi:10.1186/s40644-020-00339-6
- Abdel Razeq AAK, Helmy E. Multi-parametric arterial spin labeling and diffusion-weighted imaging in differentiation of metastatic from reactive lymph nodes in head and neck squamous cell carcinoma. *Eur Arch Otorhinolaryngol*. 2021;278:2529–2535. doi:10.1007/s00405-020-06390-0
- Fujima N, Yoshida D, Sakashita T, et al. Usefulness of pseudocontinuous arterial spin-labeling for the assessment of patients with head and neck squamous cell carcinoma by measuring tumor blood flow in the pretreatment and early treatment period. *Am J Neuroradiol*. 2016;37(2):342–348. doi:10.3174/ajnr.A4513
- Fujima N, Kudo K, Tsukahara A, et al. Measurement of tumor blood flow in head and neck squamous cell carcinoma by pseudo-continuous arterial spin labeling: comparison with dynamic contrast-enhanced MRI. *J Magn Reson Imaging*. 2015;41(4):983–991. doi:10.1002/jmri.24637

11. Lin M, Yu X, Luo D, et al. Investigating the correlation of arterial spin labeling and dynamic contrast enhanced perfusion in primary tumor of nasopharyngeal carcinoma. *Eur J Radiol*. 2018;108:222-229. doi:10.1016/j.ejrad.2018.09.034
12. Houweling AC, Schakel T, van den Berg CA, et al. MRI to quantify early radiation-induced changes in the salivary glands. *Radiother Oncol*. 2011;100(3):386-389. doi:10.1016/j.radonc.2011.08.020
13. Lee FK, King AD, Kam MK, Ma BB, Yeung DK. Radiation injury of the parotid glands during treatment for head and neck cancer: assessment using dynamic contrast-enhanced MR imaging. *Radiat Res*. 2011;175(3):291-296. doi:10.1667/RR2370.1
14. Fujita S, Hagiwara A, Hori M, et al. Three-dimensional high-resolution simultaneous quantitative mapping of the whole brain with 3D-QALAS: An accuracy and repeatability study. *Magn Reson Imaging*. 2019;63:235-243. doi:10.1016/j.mri.2019.08.031
15. Dai W, Robson PM, Shankaranarayanan A, Alsop DC. Reduced resolution transit delay prescan for quantitative continuous arterial spin labeling perfusion imaging. *Magn Reson Med*. 2012;67(5):1252-1265. doi:10.1002/mrm.23103
16. Dai W, Shankaranarayanan A, Alsop DC. Volumetric measurement of perfusion and arterial transit delay using hadamard encoded continuous arterial spin labeling. *Magn Reson Med*. 2013;69(4):1014-1022. doi:10.1002/mrm.24335
17. Maleki N, Dai W, Alsop DC. Optimization of background suppression for arterial spin labeling perfusion imaging. *MAGMA*. 2012;25(2):127-133. doi:10.1007/s10334-011-0286-3
18. Alsop DC, Detre JA, Golay X, et al. Recommended implementation of arterial spin-labeled perfusion MRI for clinical applications: A consensus of the ISMRM perfusion study group and the European consortium for ASL in dementia. *Magn Reson Med*. 2015;73(1):102-116. doi:10.1002/mrm.25197
19. Lu H, Clingman C, Golay X, van Zijl PC. Determining the longitudinal relaxation time (T1) of blood at 3.0 Tesla. *Magn Reson Med*. 2004;52(3):679-682. doi:10.1002/mrm.20178
20. Bates D, Mächler M, Bolker B, Walker S. Fitting linear mixed-effects models using lme4. *J Stat Softw*. 2015;67(1):1-48. doi:10.18637/jss.v067.i01
21. Barnhart HX, Barboriak DP. Applications of the repeatability of quantitative imaging biomarkers: a review of statistical analysis of repeat data sets. *Transl Oncol*. 2009;2(4):231-235. doi:10.1593/tlo.09268
22. Hales PW, Kawadler JM, Aylett SE, Kirkham FJ, Clark CA. Arterial spin labeling characterization of cerebral perfusion during normal maturation from late childhood into adulthood: normal 'reference range' values and their use in clinical studies. *J Cereb Blood Flow Metab*. 2014;34(5):776-784. doi:10.1038/jcbfm.2014.17
23. Zavala Bojorquez J, Bricq S, Acquitier C, Brunotte F, Walker PM, Lalande A. What are normal relaxation times of tissues at 3 T? *Magn Reson Imaging*. 2017;35:69-80. doi:10.1016/j.mri.2016.08.021
24. Abdel Razek AAK. Multi-parametric MR imaging using pseudo-continuous arterial-spin labeling and diffusion-weighted MR imaging in differentiating subtypes of parotid tumors. *Magn Reson Imaging*. 2019;63:55-59. doi:10.1016/j.mri.2019.08.005
25. Lin M, Yu X, Ouyang H, Luo D, Zhou C. Consistency of T2WI-FS/ASL fusion images in delineating the volume of nasopharyngeal carcinoma. *Sci Rep*. 2015;5:18431. doi:10.1038/srep18431
26. Chappell MA, MacIntosh BJ, Donahue MJ, Gunther M, Jezzard P, Woolrich MW. Separation of macrovascular signal in multi-inversion time arterial spin labelling MRI. *Magn Reson Med*. 2010;63(5):1357-1365. doi:10.1002/mrm.22320
27. Wheeler RH, Ziessman HA, Medvec BR, et al. Tumor blood flow and systemic shunting in patients receiving intraarterial chemotherapy for head and neck cancer. *Cancer Res*. 1986;46(8):4200-4204.
28. Herscovitch P, Raichle ME. What is the correct value for the brain-blood partition coefficient for water? *J Cereb Blood Flow Metab*. 1985;5:65-69. doi:10.1038/jcbfm.1985.9
29. Hirata K, Hattori N, Katoh C, et al. Regional partition coefficient of water in patients with cerebrovascular disease and its effect on rCBF assessment. *Nucl Med Commun*. 2011;32(1):63-70. doi:10.1097/MNM.0b013e3283412106

SUPPORTING INFORMATION

Additional supporting information can be found online in the Supporting Information section at the end of this article.

How to cite this article: Sijtsema ND, Petit SF, Verduijn GM, et al. Multidelay pseudocontinuous arterial spin labeling to measure blood flow in the head and neck. *NMR in Biomedicine*. 2023;e4898. doi:10.1002/nbm.4898